Inertial range skewness of the longitudinal velocity derivative in locally isotropic turbulence

S. Sukoriansky,[1,2,*] E. Kit,[2,3] E. Zemach,[4] S. Midya,[2] and H. J. S. Fernando[2,5]

[1]*Department of Mechanical Engineering, Ben-Gurion University of the Negev, Beer-Sheva, 84105, Israel*

[2]*Department of Civil and Environmental Engineering and Earth Sciences, University of Notre Dame, Notre Dame, Indiana 46530, USA*

[3]*School of Mechanical Engineering, Tel Aviv University, Tel Aviv 69978, Israel*

[4]*SOREQ Nuclear Research Center, Israel*

[5]*Department of Aerospace and Mechanical Engineering, University of Notre Dame, Notre Dame, Indiana 46530, USA*

(Received 7 May 2018; published 16 November 2018)

Longitudinal velocity-derivative skewness S_0 is directly proportional to the rate of enstrophy generation and hence is a key parameter for characterizing small-scale turbulence. Obtaining S_0 requires accurate measurements of the finest scales in the dissipation subrange. In this paper we define a derivative skewness of the inertial range scales that is readily accessible experimentally, and we derive its value analytically. The results depend on the filtering procedure of small scales. Analytically derived inertial range skewness is compared with those computed by high-resolution numerical simulations and obtained in laboratory and field experiments. An alternative definition of the derivative skewness in the full and the inertial range scales is examined to identify the effects of intermittency.

DOI: 10.1103/PhysRevFluids.3.114605

I. INTRODUCTION

Turbulence is a multiscale phenomenon [1]. While an accurate description of the largest fluctuating scales is needed for evaluation of transport of momentum and scalars, characterization of small-scale properties is important for understanding turbulence dynamics and developing accurate subgrid-scale (SGS) parametrizations. Difficulties in understanding dynamics at different scales stem from the strong nonlinearity of dynamic equations and intrinsic instabilities and stochastic behavior of their solutions. Thus, for progress in turbulence modeling, simplifying assumptions are made, perhaps the most prominent being the notion of universal self-similar or quasi-self-similar behavior at small scales. This concept allows us to analytically derive scaling laws and characteristic scale-dependent parameters of turbulence.

Skewness of the longitudinal velocity derivative, defined as

$$S_0 = \langle(\partial u_1/\partial x_1)^3\rangle/\langle(\partial u_1/\partial x_1)^2\rangle^{3/2}, \tag{1.1}$$

is an important parameter pertinent to small scales of turbulence. The symbol $\langle\cdot\rangle$ henceforth denotes ensemble averaging, and the subscript "0" indicates that all scales are accounted for in computation of skewness. For random noise, $S_0 = 0$, while for locally homogeneous and isotropic turbulence, the values of $-S_0$ are in the range 0.3–0.5, rising to about 0.7 for high Reynolds number data [1]. This property of skewness is used as a "quality control" criterion in turbulent velocity measurements.

*semion@bgu.ac.il

Turbulence measurements are usually embedded with a relatively high level of noise due to the use of intricate instrumentation, such as hot wires or films thermo-anemometers. In acoustic doppler current profilers, where the signal-to-noise-ratio is relatively low, the skewness can be used to separate the measured signal into "good" and "bad" events. In particular, Kit *et al.* [2] used skewness of the longitudinal velocity derivative to select appropriate events in an ensemble chosen for averaging.

The relation between the skewness and enstrophy production, and hence energy transfer down the spectrum, makes the former even more useful in turbulence studies. In homogeneous isotropic turbulence, the skewness represents the rate of enstrophy generation due to vortex stretching [3,4]. More precisely, in three-dimensional isotropic turbulence, S_0 is a nondimensional measure of the rate of enstrophy production [5]:

$$\left\langle \omega_i \omega_j \frac{\partial u_i}{\partial x_j} \right\rangle = -\frac{35}{2} S_0 \left(\frac{\varepsilon}{15 \nu_0} \right)^{3/2}. \tag{1.2}$$

Here $\boldsymbol{\omega}$ is the vorticity, $\langle \omega^2 \rangle / 2$ is the enstrophy, and ε and ν_0 are the mean turbulent kinetic energy (TKE) dissipation rate and the kinematic molecular viscosity, respectively. This equation follows directly from the relation

$$\left\langle \omega_i \omega_j \frac{\partial u_i}{\partial x_j} \right\rangle = -\frac{35}{2} \left\langle \left(\frac{\partial u_1}{\partial x_1} \right)^3 \right\rangle, \tag{1.3}$$

which is valid for isotropic turbulence [6]. Nonlinearity of the Navier-Stokes equation is necessary but not sufficient for S_0 to be nonzero, as it vanishes in the inverse cascade range of two-dimensional turbulence.

Measurement of S_0 in high Reynolds number flows is difficult, because in order to conduct this measurement, a viscous subrange must be fully and accurately resolved. In addition, while small scales are the largest contributors to S_0, the share of the larger scales is also consequential. As such, S_0 depends on the Reynolds number Re [7]. Numerical simulations and laboratory measurements at low Re do not give an accurate depiction of skewness for a very large Reynolds number fully developed turbulence because of the limited range of scales obtainable. Experimental S_0 varies over a wide range, both due to the dependence on Re and the experimental noise and because reliable measurements are not available hitherto (see Refs. [8–10] and references therein). Moreover, the noise contribution increases at high Re due to the difficulty of resolving finer scales.

Alternatively, a more easily measurable, yet versatile, parameter is the skewness of velocity derivatives within the inertial range of scales, which is defined and addressed in the following sections. Since the scaling subrange is selected, this parameter can be computed in the Fourier space. For simplicity, we start this analyses assuming the known Kolmogorov constant, C_K. More accurate derivations that do not rely on adjustable parameters will be given in Secs. VI and VII using quasi-normal-scale elimination (QNSE) theory. Intermittency effects are considered in Sec. VIII.

II. FOURIER SPACE REPRESENTATION OF S_0

For isotropic homogeneous turbulence, Eq. (1.1) can be rewritten in the Fourier space. In a statistically steady state where enstrophy production and dissipation are in balance,

$$\left\langle \omega_i \omega_j \frac{\partial u_i}{\partial x_j} \right\rangle = \nu_0 \left\langle \frac{\partial \omega_i}{\partial x_j} \frac{\partial \omega_i}{\partial x_j} \right\rangle = 2 \nu_0 \int_0^\infty k^4 E(k)\, dk, \tag{2.1}$$

where $E(k)$ is the three-dimensional energy spectrum. Recalling that in isotropic turbulence ε is related to the spectrum $E(k)$ and the one-dimensional longitudinal spectrum $E_1(k_1)$ as

$$\varepsilon = 2\nu_0 \int_0^\infty k^2 E(k)\, dk = 15\nu_0 \int_0^\infty k_1^2 E_1(k_1)\, dk_1, \tag{2.2}$$

and substituting (2.1) and (2.2) into (1.2), one gets the following spectral representations:

$$S_0 = -\frac{4}{35}\frac{\nu_0 \int_0^\infty k^4 E(k)\,dk}{\left[\int_0^\infty k_1^2 E_1(k_1)\,dk_1\right]^{3/2}} = -\frac{3\sqrt{30}}{7}\frac{\nu_0 \int_0^\infty k^4 E(k)\,dk}{\left[\int_0^\infty k^2 E(k)\,dk\right]^{3/2}}. \tag{2.3}$$

The analytical computation based on Eq. (2.3) or a similar expression depends strongly on the form of energy spectrum in the dissipation subrange, which remains uncertain.

III. INERTIAL RANGE SKEWNESS

Let $\mathbf{u}(\mathbf{x}, t)$ be the homogeneous isotropic velocity field. For any cutoff wave number k_c we define the filtered velocity field $\mathbf{u}(\mathbf{x}, t|k_c)$ as the physical space velocity with all Fourier modes $|\mathbf{k}| > k_c$ set to 0:

$$\mathbf{u}(\mathbf{x}, t|k_c) = \mathcal{F}^{-1}(\tilde{\mathbf{u}}(\mathbf{k}, t)\theta(k_c - |\mathbf{k}|)). \tag{3.1}$$

Here θ is the Heaviside step function and $\mathcal{F}^{-1}$ is the inverse Fourier transform operator. Skewness S_{kc} is defined according to (1.1) with the original velocity replaced by the filtered velocity $\mathbf{u}(\mathbf{x}, t|k_c)$. If k_c belongs to the inertial range, then both $\langle(\partial u_1/\partial x_1)^3\rangle$ and $\langle(\partial u_1/\partial x_1)^2\rangle$ should be independent of ν_0 and forcing details and should depend only on the energy injection rate ε and k_c. Then, from dimensional analysis, the dimensionless parameter S_{kc} is a constant independent of k_c.

The dynamical effect of filtered small scales can be represented by an eddy viscosity, which is introduced in such a way that the energy exchange between the eliminated and the remaining "resolvable" scales remains unchanged. The energy transfer from resolvable scales to the eliminated ones can be viewed as an energy loss due to eddy viscosity and will be kept equal to the energy dissipation rate of original turbulence by the molecular viscosity ν_0. Kraichnan [11] has shown that an effective eddy viscosity acting on resolvable modes $k < k_c$ must depend on two parameters, k and k_c. Computation of S_{kc} using Kraichnan's two-parametric eddy viscosity $\nu(k|k_c)$ will be given in Sec. VII. A simpler derivation presented in this section is based on the Kolmogorov spectrum and eddy viscosity that accounts for the dissipative action of eliminated scales on all remaining scales $k < k_c$ yet depends only on k_c. The eddy viscosity $\nu(k|k_c)$ has a cusplike form as $k \to k_c$ [11]. Ignoring the cusp, the approximate k-independent value $\nu(k_c)$ can be found from the energy balance equation

$$\varepsilon = 2\,\nu(k_c)\int_0^{k_c} k^2 E(k)\,dk. \tag{3.2}$$

Substituting the inertial range Kolmogorov spectrum $E(k) = C_K\,\varepsilon^{2/3}k^{-5/3}$ one finds

$$\nu(k_c) = \frac{2}{3C_K}\,\varepsilon^{1/3}k_c^{-4/3}. \tag{3.3}$$

For the filtered velocity $\mathbf{u}(\mathbf{x}, t|k_c)$, the enstrophy production relation (2.1) holds with the upper limit of integration replaced by k_c and the molecular viscosity ν_0 replaced by $\nu(k_c)$:

$$\left\langle \omega_i\omega_j\frac{\partial u_i}{\partial x_j}\middle| k_c\right\rangle = 2\,\nu(k_c)\int_0^{k_c} k^4 E(k)\,dk = \frac{2}{5}\varepsilon k_c^2. \tag{3.4}$$

Let us now derive the filtered field equivalence of the denominator in Eq. (1.1). The spectral tensor of the solenoidal isotropic field is [4]

$$F_{ij}(\mathbf{k}) = \frac{E(k)}{4\pi k^2}\left(\delta_{ij} - \frac{k_i k_j}{k^2}\right). \tag{3.5}$$

Integrating $k_1^2 F_{11}(\mathbf{k})$ over the sphere of radius k_c we obtain the required relation:

$$\left\langle \left[\frac{\partial u_1(\mathbf{x}|k_c)}{\partial x_1} \right]^2 \right\rangle = \frac{1}{10} C_K \varepsilon^{2/3} k_c^{4/3} \tag{3.6}$$

The inertial range skewness S_{kc} can now be computed using, (1.3), (3.4) and (3.6) with the result

$$S_{kc} = -\frac{8\sqrt{2/5}}{7C_K^{3/2}}. \tag{3.7}$$

The same result can be obtained using the modified Eq. (2.3), with the upper limit of integration replaced by k_c and the molecular viscosity ν_0 replaced by $\nu(k_c)$. For the Kolmogorov constant C_K value belonging to the interval between 1.5 and 1.7, the value of S_{kc} is between -0.393 and -0.326. This result will be verified in Sec. V using direct numerical simulations.

IV. INERTIAL RANGE SKEWNESS IN ONE-DIRECTIONAL FILTERING

The inertial range skewness defined above can be assessed using laboratory data if the total turbulent field is measured. However, usually this is not obtained in field experiments where only longitudinal spectral components are collected by a hot-wire probe. In this case, a different derivation of inertial range skewness is needed.

We start from the derivation of the equation for S_0 utilizing the Von Karmán-Howarth-Kolmogorov equation (VKHK) written in physical space ([12,13]). The VKHK equation is an exact dynamical relation which can be derived from the Navier-Stokes equations for isotropic turbulence [4],

$$D_{LLL}(r) - 6\nu_0[dD_{LL}(r)/dr] = -4/5\,\varepsilon r. \tag{4.1}$$

Here $D_{LL}(r)$ and $D_{LLL}(r)$ are the second- and the third-order velocity structure functions, respectively:

$$D_{LL}(r) = \langle [u_1(x_1 + r) - u_1(x_1)]^2 \rangle, \tag{4.2}$$

$$D_{LLL}(r) = \langle [u_1(x_1 + r) - u(x_1)]^3 \rangle. \tag{4.3}$$

Nelkin [13] derived an equation for S_0 using the Taylor expansion of Eq. (4.1), which, in terms of order r, gives the energy dissipation

$$\varepsilon = 15\nu_0 \langle (\partial u_1/\partial x_1)^2 \rangle, \tag{4.4}$$

while the terms of order r^3 express the balance between enstrophy production and dissipation:

$$\langle (\partial u_1/\partial x_1)^3 \rangle = -2\,\nu_0 \langle (\partial^2 u_1/\partial {x_1}^2)^2 \rangle. \tag{4.5}$$

The last relation allows one to rewrite the skewness S_0 in spectral form:

$$S_0 = -2\,\nu_0 \langle (\partial^2 u_1/\partial {x_1}^2)^2 \rangle / \langle (\partial u_1/\partial x_1)^2 \rangle^{3/2} = -2\,\nu_0 \int_0^\infty {k_1}^4 E_1(k_1)\,dk_1 \Big/ \left[\int_0^\infty {k_1}^2 E_1(k_1)\,dk_1 \right]^{3/2}. \tag{4.6}$$

Let $u_1(k_1, x_2, x_3, t) = \int u_1(x_1, x_2, x_3, t)\, \exp(-ik_1 \cdot x_1)\, dx_1$ be the one-dimensional Fourier transform of the velocity component u_1. For a cutoff wave number k_{1c}, we now define the filtered velocity component $u_1(\mathbf{x}, t|k_{1c})$ as the physical space velocity with all Fourier modes $|k_1| > k_{1c}$ set to 0. The skewness S_{1c} is defined according to (1.1) with the original velocity replaced by the filtered velocity $u_1(\mathbf{x}, t|k_{1c})$.

The one-directional filtering destroys the isotropy of the remaining resolvable modes, which significantly complicates the derivations. Still, derivations similar to those that resulted in (4.6) and based on structure functions (4.2, 4.3) can be employed in order to compute inertial range skewness S_{1c}. Modification is needed since filtering out of modes $|k_1| > k_{1c}$ generates the eddy viscosity $\nu_1(k_{1c})$ that replaces the bare viscosity ν_0. Note, that the "eddy viscosity" $\nu_1(k_{1c})$ results from the elimination of modes with only the first component of the vector $\mathbf{k}$ larger than k_{1c}. It is different from the isotropic eddy viscosity (3.3) obtained by scale elimination of all modes with $|\mathbf{k}| > k_c$. We also ignore a possible cusplike behavior of the corresponding two-parametric viscosity.

An expression for $\nu_1(k_{1c})$ can be derived using the energy balance equation that accounts for the fact that the energy "loss" based on the eddy viscosity is equal to the energy dissipation rate of the original turbulence at molecular scales:

$$\varepsilon = 15\nu_1(k_{1c})\int_0^{k_{1c}} k_1^2 E_1(k_1)\,dk_1, \tag{4.7}$$

where the longitudinal energy spectrum $E_1(k_1)$ is

$$E_1(k_1) = (18/55)\,C_K\varepsilon^{2/3}k_1^{-5/3}. \tag{4.8}$$

Substituting (4.8) into (4.7), we obtain

$$\nu_1(k_{1c}) = \frac{22}{81\,C_K}\,\varepsilon^{1/3}k_{1c}^{-4/3}. \tag{4.9}$$

We now define the second- and the third-order longitudinal velocity structure functions of the filtered velocity component $u_1(\mathbf{x}, t|k_{1c})$:

$$\widetilde{D}_{LL}(r) = \langle[u_1(x_1 + r|k_{1c}) - u_1(x_1|k_{1c})]^2\rangle, \tag{4.10}$$

$$\widetilde{D}_{LLL}(r) = \langle[u_1(x_1 + r|k_{1c}) - u_1(x_1|k_{1c})]^3\rangle. \tag{4.11}$$

After filtering, the left-hand side of Eq. (4.1) becomes $\widetilde{D}_{LLL}(r) - 6\nu_1(k_{1c})[d\widetilde{D}_{LL}(r)/dr]$. At large separation distances $r \gg 1/k_{1c}$, the viscous term in this expression is negligibly small and the remaining third-order structure function approaches the Kolmogorov limit $\widetilde{D}_{LLL}(r) \to -4/5\varepsilon r$. Assuming that the separation distance r is infinitesimally small, it is possible to compute the Taylor series decomposition:

$$\begin{aligned}\widetilde{D}_{LLL}(r) - 6\nu_1(k_{1c})[d\widetilde{D}_{LL}(r)/dr] &= -12\,\nu_1(k_{1c})\langle[\partial u_1(x_1|k_{1c})/\partial x_1]^2\rangle r \\ &= -4/5\varepsilon r + O(r^3).\end{aligned} \tag{4.12}$$

In this derivation, we routinely imposed the condition of flow homogeneity. The final result is identical to the Taylor series decomposition of Eq. (4.1) with the exception that ν_0 in this decomposition is replaced by $\nu_1(k_{1c})$, given by (4.9). The same is true also for the next $O(r^3)$ term, which has the form $(\langle[\partial u_1(x_1|k_{1c})/\partial x_1]^3\rangle + 2\,\nu_1(k_{1c})\langle[\partial^2 u_1(x_1|k_{1c})/\partial {x_1}^2]^2\rangle)r^3$. Note that the filtered field remains homogeneous and isotropic on scales $|\mathbf{k}| < k_{1c}$, and that Eq. (4.12) has the same asymptotic value $-4/5\varepsilon r$ at large and small r as the original VKHK equation. We therefore infer that the VKHK equation remains intact also for the filtered velocity if the molecular viscosity is replaced by $\nu_1(k_{1c})$. Thus, the coefficient in the r^3 term of (4.12) is equal to zero, which leads to the filtered field analog of Eq. (4.5):

$$\langle[\partial u_1(x_1|k_{1c})/\partial x_1]^3\rangle = -2\,\nu_1(k_{1c})\langle[\partial^2 u_1(x_1|k_{1c})/\partial {x_1}^2]^2\rangle. \tag{4.13}$$

Equation (4.13) yields the inertial range skewness S_{1c} in the form

$$S_{1c} = -\frac{2\,\nu_1(k_{1c})\langle[\partial^2 u_1(x_1|k_{1c})/\partial {x_1}^2]^2\rangle}{\langle[\partial u_1(x_1|k_{1c})/\partial x_1]^2\rangle^{3/2}} = -\frac{2\,\nu_1(k_{1c})\int_0^{k_{1c}} k_1^4 E_1(k_1)\,dk_1}{\left[\int_0^{k_{1c}} k_1^2 E_1(k_1)\,dk_1\right]^{3/2}}. \tag{4.14}$$

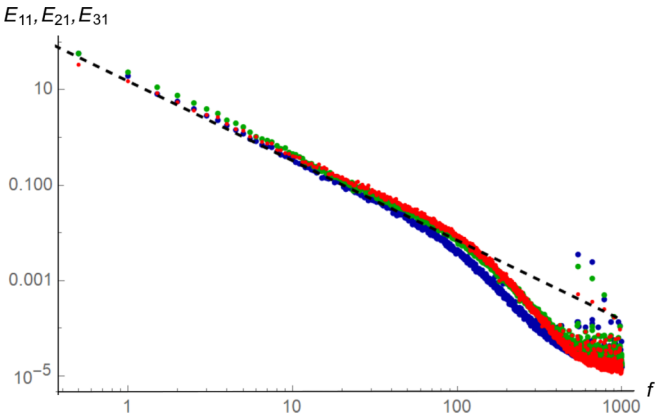

FIG. 1. One-dimensional spectra of three velocity components, u (blue), v (green), and w (red); the dashed line corresponds to the Kolmogorov $-5/3$ spectrum.

Finally, substituting (4.8) and (4.9) into (4.14), we get

$$S_{1c} = -\frac{88}{243}\sqrt{\frac{22}{15}}C_K^{-3/2}. \tag{4.15}$$

As expected, the inertial range skewness is independent of the cutoff wave number k_{1c}. For the Kolmogorov constant C_K value between 1.5 and 1.7, S_{1c} is between -0.239 and -0.198. These values are smaller than the values of S_{kc} [Eq. (3.7)] by the factor 1.648. In the next section, we use large Reynolds number and high-resolution atmospheric and laboratory measurements to verify this analytical prediction.

V. COMPUTATION OF SKEWNESS FROM ATMOSPHERIC MEASUREMENTS, LABORATORY EXPERIMENTS, AND NUMERICAL SIMULATIONS

Atmospheric measurements conducted during the MATERHORN campaign were used to compute the inertial range skewness S_{1c}. The campaign was conducted at the Granite Mountain Atmospheric Sciences Test Bed (GMAST) of the U.S. Army Dugway Proving Ground (DPG), Utah (for details, see Refs. [14,15]). In one of the 32-m-high flux towers of MATERHORN, a double-combo system was mounted at a height of 6 m, and this tower was a part of the densely instrumented flux tower array, designed to study stable stratified downslope (katabatic) flows at night on the eastern slope of the Granite Mountain. The combo systems and associated turbulence measurements are described in Ref. [9]. In this system, multi-hot-wire probes were embedded into the measured volume of a collocated sonic anemometer. Such a dyad ("combo") enables in-situ calibration of a hot-film probe, as was discussed in Refs. [9,16].

As explained in Ref. [9], some data periods include burst events that may affect the skewness. Therefore, the data intervals that do not contain bursts were chosen first. The data contain 9 min of velocity measurements with a sampling rate of 2000 Hz. This allowed dealing with velocity fluctuations for frequencies up to 1000 Hz (Nyquist frequency). The total length included 1 080 000 data points for every velocity component. Each array was partitioned on nine pieces, with each piece containing 1 min of measurements. The partition was used for ensemble averaging.

The kinetic energy spectra of all three velocity components (u, v, w) are shown in Fig. 1. Components u and v are horizontal and w is vertical, and u is in the mean wind direction. The Taylor frozen turbulence hypothesis was employed in spectral computations, and the frequency-dependent spectra are shown. It is possible to transform the frequency to the wave number k_x using the longitudinal average wind speed U as

$$k_x = 2\pi f/U. \tag{5.1}$$

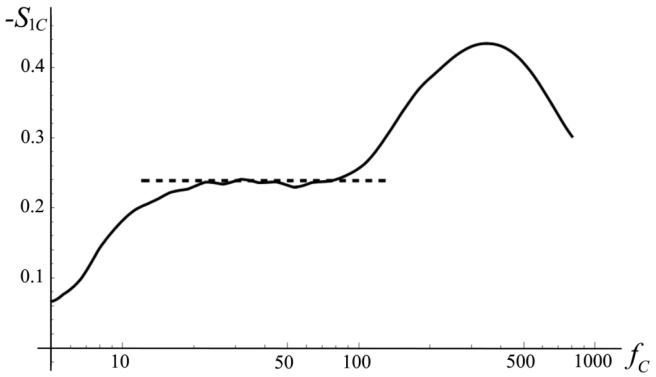

FIG. 2. Scale-dependent skewness S_{1c} as a function of the cutoff frequency f_c. The analytical value 0.24 is shown by a dashed line.

A well-defined inertial range is evident over almost two decades of frequences $1 < f < 100$ Hz. The dissipation range at $f > 100$ Hz is also well resolved. Note that the Taylor microscale is $\lambda = 0.1$ m, which corresponds to the frequency 40 Hz. The Taylor microscale Reynolds number is $R_\lambda \approx 1250$.

For every cutoff frequency f_c, the f_c-dependent skewness was computed using the following steps: in the Fourier transformed longitudinal velocity $\tilde{u}(f)$, all the frequency modes outside of the interval $-f_c < f < f_c$ are set to 0; then the inverse Fourier transform of the filtered velocity $\tilde{u}(f|f_c)$ is taken and the filtered velocity $u(t|f_c)$ is obtained in the physical space; the time derivative $\partial u(t|f_c)/\partial t$ is calculated and substututed in the following formula, which leads to the final result:

$$S_{1c} = -\frac{\langle[\partial u(t|f_c)/\partial t]^3\rangle}{\langle[\partial u(t|f_c)/\partial t]^2\rangle^{3/2}}. \tag{5.2}$$

Use of the Taylor hypothesis allows the time derivative of a single-point measurement to be related to the spatial derivative as

$$\frac{\partial u}{\partial t} = -U\frac{\partial u}{\partial x}. \tag{5.3}$$

Substitution of (5.3) into (5.2) confirms that (5.2) is identical to the k_{1c}-dependent skewness S_{1c} defined in the previous section.

The scale-dependent skewness is shown in Fig. 2. In the inertial range $10 < f_c < 100$ Hz, the measured skewness is almost identical to the theoretical prediction. The gradual decrease of the skewness at $f_c < 10$ Hz is due to the effect of large scales that do not belong to the inertial range.

In order to clarify the large-scale influence, we computed skewness at the cutoff frequency $f_c = 85$ Hz from the filtered data in which, in addition to high-frequency modes $|f| > f_c$, low-frequency modes $|f| < f_l$ were also removed. The result is shown in Fig. 3 as a function of f_l. If all low-frequency modes are kept ($f_l = 0$), the skewness is very close to the theoretical value -0.24. With increasing low-frequency cutoff, the skewness remains almost constant up to $f_l \approx 2$. Above this value, the skewness decreases with increasing f_l until it approaches 0 at $f_l \to f_c$. Thus, we conclude that the skewness is not a local parameter: almost two decades of inertial range modes below the given frequency f_c contribute to S_{1c}.

A. Laboratory measurements: Turbulent jet

The results from the jet facility [16] were employed for computations of skewness in the inertial range. The jet facility used was a multipurpose calibration rig. It was used to obtain a

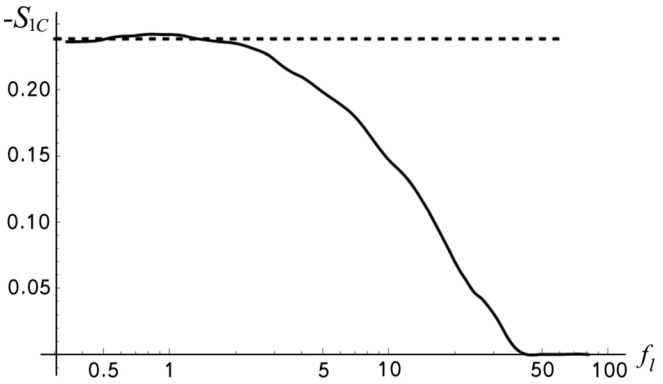

FIG. 3. Scale-dependent skewness at $f_c = 85\,\text{Hz}$ as a function of the low-frequency cutoff f_l. Analytical value (0.24) is shown as a dashed line.

canonical turbulent (jet) flow in the laboratory and also as a calibrator in the field. The laboratory measurements may have some advantages in comparison with field experiments. The mean jet direction and velocity are known, and temperature variations are minimal in the laboratory. In the field, however, the wind velocity and direction are variable depending on the larger-scale forcing conditions.

The custom-made calibration unit consisted of a computer-controlled blower, connected to a settling chamber followed by a contraction with a cross-section ratio approximately 11 and exit nozzle diameter $D_e = 38.1\,\text{mm}$. The same facility was used to measure all three components of turbulent velocity at various downstream cross sections. For more details, see Ref. [16].

Spectra in this case are not isotropic (not shown) and have only a very short inertial range (Fig. 4). Skewness, accordingly, is close to the theoretical value of 0.24 only in a very short frequency interval (Fig. 5).

B. Numerical simulations

Skewness of the longitudinal velocity derivative from inertial to dissipation ranges of three-dimensional (3D) homogeneous steady turbulent flow was studied using a high-resolution direct

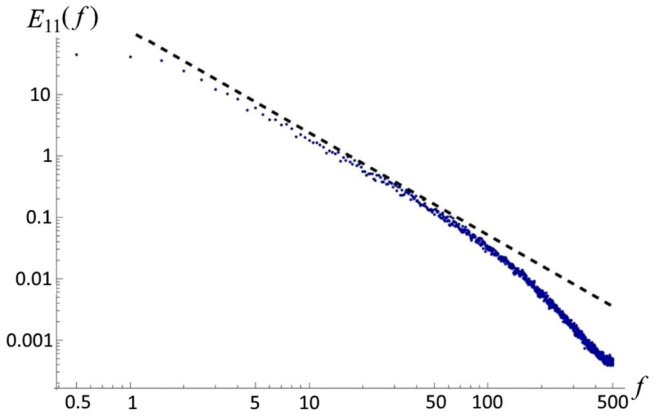

FIG. 4. One-dimensional spectrum of horizontal velocity component in the jet experiment; the dashed line corresponds to the Kolmogorov $-5/3$ spectrum.

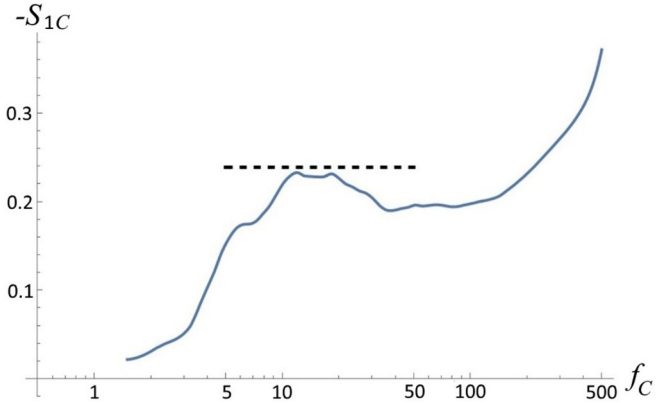

FIG. 5. Scale-dependent skewness S_{1c} in the jet experiment as a function of the cutoff frequency f_c. Analytical value (0.24) is shown as a dashed line.

numerical simulation (DNS) with 1024^3 grid points. A pseudospectral code with large-scale random forcing and triply periodic boundary conditions was used. The white in time Gaussian forcing was placed in the range of scales $1 \leqslant k \leqslant \sqrt{6}$. Details of the numerical scheme can be found in Ref. [17]. The Taylor microscale Reynolds number R_λ was 380.

The 3D energy spectrum is presented in Fig. 6. The spectrum has a well-developed inertial range of $3 < k < 80$ with a Kolmogorov constant of $C_K = 1.64$. Skewness parameters S_{kc} and S_{1c}, shown in Fig. 7, are very close to theoretical values in the inertial range, except at scales near the forcing scale. In the dissipation range when all scales are resolved, the absolute value of skewness is larger, close to 0.6, which indicates that energy dissipation decreases here more rapidly than enstrophy production.

VI. QNSE THEORY AS AN EFFICIENT TOOL TO COMPUTE INERTIAL RANGE PROPERTIES: SHORT DESCRIPTION OF THE QNSE METHODOLOGY

Inertial range skewness (3.7) derived in Sec. III relies on the assumption of the one-parametric eddy viscosity $\nu(k_c)$ and strongly depends on the empirical Kolmogorov constant C_K. In this section we use quasi-normal-scale elimination (QNSE) theory [18,19] to remove these restrictions. The QNSE method utilizes the Fourier transformed equations of motion and is well suited for calculating inertial range parameters. The major difficulty, however, is the fact that the momentum equation becomes strongly nonlinear as the Reynolds number increases with increase of scale. The situation

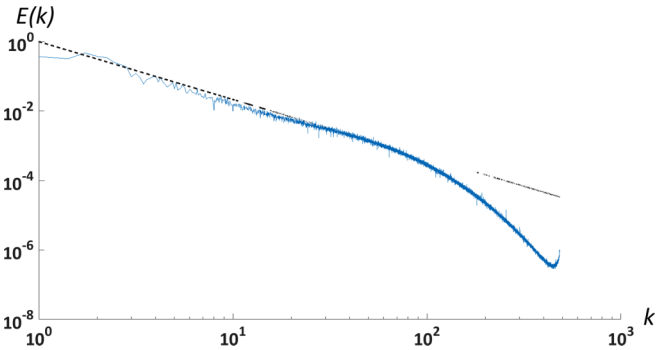

FIG. 6. Three-dimensional energy spectrum computed in DNS.

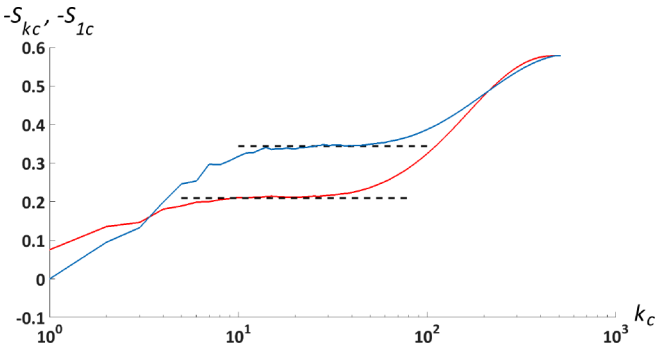

FIG. 7. Scale-dependent skewness S_{kc} (blue) and S_{1c} (red) obtained in the DNSs as a function of the cutoff wave number. Analytical values corresponding to Eqs. (3.7) and (4.15) are shown as dashed lines.

is different near the dissipation scales where the linear and nonlinear effects are comparable. In other words, the scale-dependent Re is $O(1)$ on these scales. The smallness of Re allows one to apply a renormalized perturbation method operating with a "dressed" or "effective" eddy viscosity, rather than with the "bare" molecular value. The QNSE method employs gradual coarsening of the turbulent field by successive averaging over small shells Δk of Fourier modes adjacent to moving dissipation cutoff k_c (shell elimination procedure). The averaging generates small $O(\Delta k)$ correction to the viscosity that accounts for the transport processes that take place on the eliminated scales. With the increase of effective viscosity, the effective dissipation wave number k_c also decreases. The effective Re built upon the scales pertinent to the new value of k_c is again $O(1)$, thus making it possible to repeat the procedure. Taking the limit $\Delta k \to 0$, one obtains a differential equation relating the effective viscosity to the current value of k_c. The effective k_c-dependent (eddy) viscosity resulting from this procedure can be used as a SGS viscosity in large eddy simulations, where k_c is determined by the grid resolution [20–22]. The algorithm of successive small scale elimination was initially developed within the renormalization group theory of turbulence (RNG) [18,23–26], but it differs from RNG because it uses neither the ε expansion nor the fixed-point arguments. Instead, the QNSE theory relies upon the assumption of quasinormality within the shell Δk. The QNSE method has been applied to various turbulent flows such as isotropic homogeneous turbulence with no extra strains [18], stably stratified flow [19], turbulent magneto-hydrodynamic flow [28], and turbulent flow in a rotating frame [27]. In the case of neutral flow, the QNSE theory recovers the RNG results, yielding the classical Kolmogorov and Corrsin-Obukhov spectra of the kinetic energy and temperature fluctuations and their respective universal constants. According to this theory, the wave number-dependent eddy viscosity $\nu(k_c)$ is

$$\nu(k_c) \approx 0.46\, \varepsilon^{1/3} k_c^{-4/3}. \tag{6.1}$$

The eddy viscosity (6.1) is calculated using the "distant interaction" or "spectral gap" approximation [27]. In this computation only the terms up to $O[(k/k_c)^2]$ are retained. This is equivalent to introducing a virtual spectral gap between resolvable and eliminated scales and taking the renormalized viscosity acting on the scales $k \in (0,\ k_c)$ constant and equal to their values at k_c. The three-dimensional energy spectrum $E(k)$ in a neutral flow derived within the QNSE framework [19] is

$$E(k) = C_K\, \varepsilon^{2/3} k^{-5/3}, \tag{6.2}$$

with $C_K \approx 1.5$.

In the next section we introduce a correction to this value and derive the actual two-parametric eddy viscosity $\nu(k|k_c)$ accounting for the effect of the eliminated scales on different resolvable scales k.

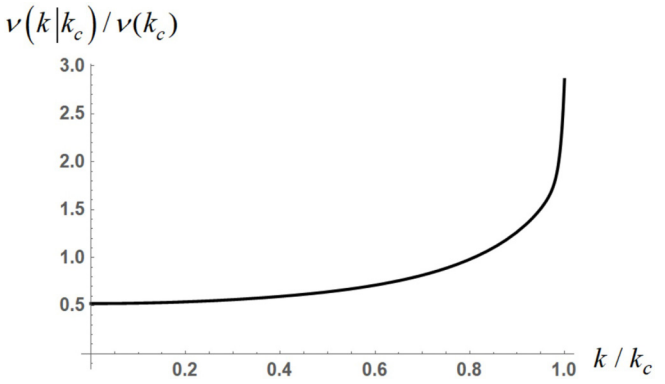

FIG. 8. Normalized two-parametric viscosity.

VII. COMPUTATION OF INERTIAL RANGE SKEWNESS USING QNSE RESULTS AND TWO-PARAMETRIC EDDY VISCOSITY

Kraichnan [11] has shown that an effective eddy viscosity acting on resolvable modes $k < k_c$ must depend on two parameters, k and k_c, and may be defined as

$$\nu(k|k_c) = -\frac{T(k|k_c)}{2k^2E(k)}, \quad k < k_c, \tag{7.1}$$

where $T(k|k_c)$ is the energy transfer rate from mode k to all eliminated modes $k > k_c$. The transfer function $T(k|k_c)$ obeys the detailed conservation condition, wherein any triad satisfying $\mathbf{k}+\mathbf{p}+\mathbf{q}=0$ exchanges energy among their members conservatively. In a wide class of quasinormal spectral closures, [11,29] the triad interaction is given by the integral

$$T(k|k_c) = \iint_{\triangle} \frac{k}{p\,q}\theta_{kpq}b_{kpq}[k^2E(p) - p^2E(k)]E(q)\,dp\,dq. \tag{7.2}$$

Here the integration $\iint_{\triangle}$ signifies p and/or $q > k_c$, $b_{kpq} = \frac{p}{q}(xy + z^3)$, x, y, z are cosines of interior angles opposite k, p, q, respectively, and θ_{kpq} is the triad relaxation time. Different spectral closure models provide different expressions for θ_{kpq}. We compute θ_{kpq} using the QNSE theory:

$$\theta_{kpq} = \frac{1}{\nu(k)k^2 + \nu(p)p^2 + \nu(q)q^2}, \tag{7.3}$$

where $\nu(k)$ is given by (6.1).

The normalized two-parametric viscosity $\nu(k|k_c)/\nu(k_c)$ is presented in Fig. 8 as a function of k/k_c. One can see that this function has a cusp at k approaching k_c.

The two-parametric viscosity $\nu(k|k_c)$ was tested in DNSs of homogeneous isotropic 3D turbulence in a triply periodic box with 512^3 nodes. The molecular viscosity was replaced by $\nu(k|k_c)$ with $k_c = 240$. The energy spectrum $E(k)$ of the simulated velocity field is shown in Fig. 9. The $-5/3$ scaling is clearly seen in the whole range of resolvable scales.

The inertial range skewness S_{kc} can be computed using the modified Eq. (2.3) with molecular viscosity ν_0 replaced by $\nu(k|k_c)$:

$$S_{kc} = -\frac{4}{35}\frac{\int_0^{k_c} k^4\nu(k|k_c)E(k)\,dk}{\left[2/15\ \int_0^{k_c} k^2E(k)\,dk\right]^{3/2}} \approx -0.46. \tag{7.4}$$

The absolute value of this parameter is larger than 0.39 derived in Sec. III using the one-parametric viscosity [Eq. (3.7) with $C_K = 1.5$]. This is because the cusp in the two-parametric

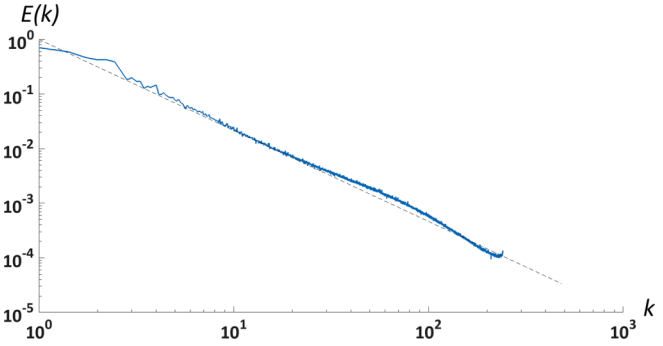

FIG. 9. 3-D spectrum obtained using DNSs with the two-parametric viscosity. Note the $-5/3$ shape in the entire spectral range.

viscosity increases the contribution of the third moment of $\partial u_1/\partial x_1$ relative to its second moment. The DNS results shown in Sec. V support a smaller value $|S_{kc}| = 0.39$. However, the DNS results are pertinent to a relatively small Re number. A higher resolution DNS with high Re numbers is needed to verify which of these results is more reliable. Note that S_{kc} in (7.4) is close to -0.49 derived using the RNG method [25]. Recall, that while being conceptually close to the RNG theory, the QNSE derivations of skewness do not employ the ε expansion and distant interaction approximation, according to which the "renormalized" parameters are computed at $k \to 0$.

VIII. INTERMITTENCY EFFECTS

Data obtained in the atmosphere and laboratory and in numerical simulations show that the skewness S_0 depends on the Reynolds number [7]. Measurements over a wide range of R_λ [30] indicate that S_0 first increases with R_λ up to $R_\lambda = 700$ and then plateaus. Such behavior can be explained by the influence of fluctuations of the rate of local turbulent energy dissipation on higher-order structure functions at small separation distances r [31]. However, in more recent experiments in wind tunnels [32], the transition at $R_\lambda = 700$ has not been observed, wherein S_0 continued to increase slowly with R_λ, although a good agreement was noted with previous experiments for $R_\lambda < 400$.

Owing to intermittency effects, as the Reynolds number increases, the distribution of velocity derivatives tends to become increasingly flatter with rising "tails" [33]. Skewness, defined as the third-order moment of velocity derivative normalized by the second-order moment, mixes moments of different orders, and thus may increase with R_λ. A reviewer suggested a different form of skewness,

$$\tilde{S} = \langle(\partial u_1/\partial x_1)^3\rangle/\langle|\partial u_1/\partial x_1|^3\rangle, \tag{8.1}$$

which is worthy of examination.

For brevity, let us denote the velocity increment $\Delta u_r = u(x + r) - u(x)$ by X (we will use the same notation also for the longitudinal derivative assuming infinitesimal r). Consider the normalized pth-order moment of $|X|$:

$$H_p^* = \frac{\langle|X|^p\rangle}{(\langle X^2\rangle)^{p/2}}. \tag{8.2}$$

The conventional pth-order moment of X can be written in the form

$$H_p = \frac{\langle X^p\rangle}{(\langle X^2\rangle)^{p/2}} = \frac{\langle X^p\rangle}{\langle|X|^p\rangle} H_p^*. \tag{8.3}$$

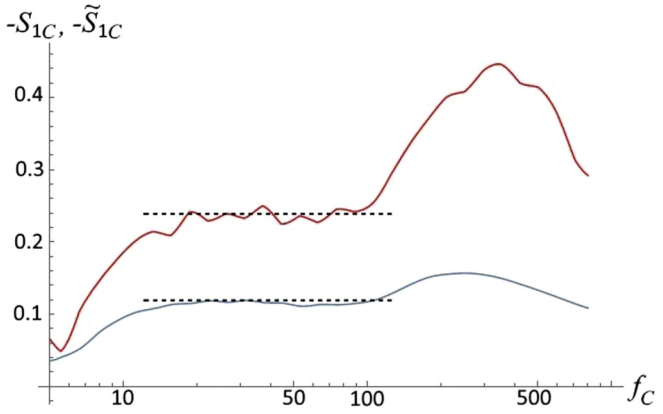

FIG. 10. Comparison of old (red) and new (blue) scale-dependent skewness S_{1c} and $\tilde{S}_{1c}$ calculated using MATERHORN data as a function of the cutoff frequency f_c. The inertial subrange values are shown by dashed lines.

H_p depends on R_λ due to the intermittency effect. For even p, the factor $\langle X^p\rangle/\langle|X|^p\rangle = 1$ and the intermittency effect is imbedded in H_p^*. It is reasonable to assume that for any real p, H_p^* alone carries the effects of intermittency. This conjecture is supported by the fact that the factor $\langle X^p\rangle/\langle|X|^p\rangle$ in (8.3) weights both X^p and $|X|^p$ for the same values of X within its probability distribution function $P(X)$, thus presumably eliminating the intermittency effect. It is also supported by the results presented in Ref. [34], which indicate that H_3 and H_3^* behave similarly with respect to dependence on R_λ.

The ratio $S_0/\tilde{S} = H_3^*$ represents the normalized third-order moment of $|\partial u_1/\partial x_1|$. As follows from the above, H_3^* can be considered as an appropriate "intermittency descriptor (sifter)," and therefore the new skewness $\tilde{S}$ is expected to be less affected by intermittency. We computed the scale-dependent values $\tilde{S}_{kc}$ and $\tilde{S}_{1c}$ of the redefined skewness using small-scale filtering procedures described in Secs. III and IV. Comparison of S_{1c} and $\tilde{S}_{1c}$ computed from the atmospheric data collected during the MATERHORN campaign are shown in Fig. 10. Figure 11 compares S_{1c} with $\tilde{S}_{1c}$ and S_{kc} with $\tilde{S}_{kc}$, based on 1024^3 resolution DNSs at $R_\lambda = 380$.

In all cases in the inertial subrange, the newly defined values are smaller than the conventional ones approximately by a factor of 2. When all modes are taken into account, including the

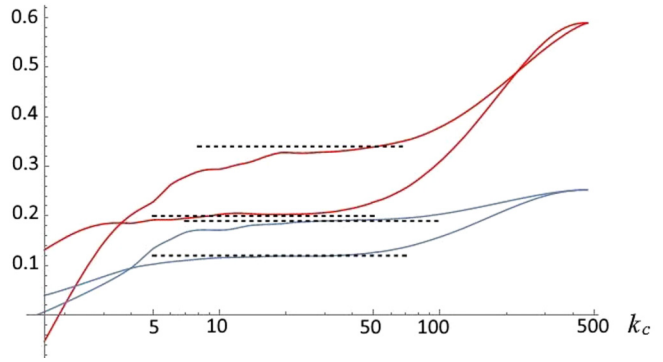

FIG. 11. Comparison of old (red) and new (blue) DNS-derived scale-dependent skewness S_{1c}, $\tilde{S}_{1c}$, S_{kc}, and $\tilde{S}_{kc}$ as functions of the cutoff wave number k_c. The inertial subrange values of each parameter are shown by dashed lines.

dissipation range scales, the ratio grows to approximately 2.5. As explained above, this ratio is determined by the intermittency descriptor $H_3^* = \langle|\partial u_1/\partial x_1|^3\rangle/\langle(\partial u_1/\partial x_1)^2\rangle^{3/2}$. The value of this factor for a Gaussian random variable is about 1.6, lower than the values of H_3^* computed both from the filtered ($\sim$2) and original flow fields ($\sim$2.5). Further high-quality experiments in the atmospheric boundary layer and high-resolution DNSs are necessary to establish the dependence of the skewness factor on R_λ and to investigate whether H_3^* enables to completely separate the effects of intermittency.

IX. CONCLUDING REMARKS

The skewness of the longitudinal velocity derivative is directly related to the enstrophy production and therefore is an important parameter for describing turbulence. In addition, the skewness is used for qualitative assurance of turbulence measurements, for example, level of noise and unsteadiness. Measurement of skewness requires accurate measurements at the finest scales in the dissipation subrange, which is an onerous task. In this paper, a derivative skewness of the inertial range scales that is conducive for measurements was introduced and its value was derived analytically using one-parametric and more accurate two-parametric eddy viscosities. The assumption of local isotropy enabled obtaining exact relations for the case where all modes with their wave number amplitude greater than a cutoff k_c were set to zero. In the case of one-dimensional (1D) filtering, which is more appropriate when field measurements are considered, the filtered form of the VKHK equation was employed. The experimentally determined values of the inertial range skewness were in very good agreement with the theoretical prediction based on the assumption of isotropy.

When fine scales of the order of the Kolmogorov scale are accurately resolved, the skewness can be computed straightforwardly. In the current study we used high-quality data collected during the MATERHORN field campaign, laboratory experiments, and DNSs. The MATERHORN data were obtained under nocturnal conditions in a mountain terrain, but stratification therein was weak. An obvious advantage is that these data belong to high Reynolds numbers typical of environmental turbulence, and the Taylor microscale R_λ of the field data used was of the order of 1300. On the other hand, the necessity of using robust high-resolution probes in this natural environment required the use of relatively large, multisensor-hot-film probes (few millimeters) that limit the measurement resolution at fine scales. To circumvent this limitation, the derivative skewness determined for the inertial range was used. There are notable advantages of using this special skewness: (1) no necessity to resolve fine scales, (2) can be estimated analytically by employing very general assumptions, and (3) in the inertial subrange, this newly defined skewness is not dependent on the cutoff frequency.

Additionally, isotropic turbulence was simulated numerically at relatively high resolution (1024^3) in a triply periodic box using DNSs. A fairly well-developed inertial range with a Kolmogorov constant $C_K = 1.64$ was obtained. The skewness was computed using 3D and 1D filtering of the velocity fields. The values computed for the inertial range were close to the theoretical prediction corresponding to $C_K = 1.64$, but slightly lower than the value derived from the MATERHORN data. The difference may indicate that the computational resolution of DNSs is not sufficient.

The two-parametric eddy viscosity was derived using QNSE modeling. To check the validity, it was implemented in DNS computations. The resulting spectra were of Kolmogorov type in the whole range of wave numbers smaller than the cutoff k_c and sharply dropped to 0 at values higher than the cutoff. The skewness in the inertial range obtained using the two-parametric viscosity was $S_{kc} = -0.46$. This is higher than the DNS-derived value. The reason for this difference is unclear, and future studies should examine whether it is due to insufficient DNS resolution or the deficiencies of the two-parametric viscosity used. The accurate value of the inertial subrange skewness can be used for quality assurance of DNS data, to determine how close the simulations represent the correct turbulent velocity field.

In numerical simulations with R_λ up to 380, the dependence of inertial range skewness on R_λ was not observed. It is known that intermittency is stronger on dissipative scales than in the inertial

range. Also, the effect of intermittency is strong for high-order moments and relatively mild for third-order moments. Therefore, the inertial range skewness is expected to weakly depend on R_λ. This conjecture needs to be examined in future studies.

The inertial range skewness is different from the normalized third-order structure function $D_{LLL}(r)/[D_{LL}(r)]^{3/2}$ computed at a large separation r [35–37]. At large r the viscous term in the VKHK Eq. (4.1) can be neglected, the third-order structure function $D_{LLL}(r)$ approaches the Kolmogorov $-4/5$ limit and $D_{LLL}(r)/[D_{LL}(r)]^{3/2} \to -0.28$. The inertial range skewness S_{1c}, on the other hand, is computed at infinitesimally small r using the filtered VKHK Eq. (4.12), where the "renormalized" eddy viscosity plays the dominant role.

Real turbulent flows are often affected by external body forces such as buoyancy and Coriolis forces that act differently on different scales. The derivative skewness of the filtered velocity field with moving filtration cutoff k_c may shed light on modification of spectral energy transport and vorticity dynamics by external forces.

ACKNOWLEDGMENTS

The results presented were obtained during the MATERHORN Program that was funded by the Office of Naval Research Award No. N00014-11-1-0709. S.S. and E.K. were also supported by the Israel Science Foundation (Grant No. 408/15), and H.J.S.F. acknowledges the support of the U.S. National Science Foundation (Grant No. AGS-1565535). We thank one of the referees, who raised important fundamental issues pertinent to moments and intermittency, and some of the referee's thoughts are reflected in this paper.

[1] U. Frisch, *Turbulence: The Legacy of AN Kolmogorov* (Cambridge University Press, Cambridge, UK, 1995).
[2] E. Kit, H. J. S. Fernando, and J. A. Brown, Experimental examination of Eulerian frequency spectra in zero-mean-shear turbulence, Phys. Fluids **7**, 1168 (1995).
[3] P. Davidson, *Turbulence: An Introduction for Scientists and Engineers* (Oxford University Press, New York, 2004).
[4] A. S. Monin and A. M. Yaglom, *Statistical Fluid Mechanics, Vol. 2: Mechanics of Turbulence* (Courier Corporation, Indianapolis, 2013).
[5] G. K. Batchelor and A. A. Townsend, Decay of vorticity in isotropic turbulence, Proc. R. Soc. London A **190**, 534 (1947).
[6] F. H. Champagne, The fine-scale structure of the turbulent velocity field, J. Fluid Mech. **86**, 67 (1978).
[7] K. R. Sreenivasan and R. A. Antonia, The phenomenology of small-scale turbulence, Annu. Rev. Fluid Mech. **29**, 435 (1997).
[8] E. Kit and D. Liberzon, 3D-calibration of three-and four-sensor hot-film probes based on collocated sonic using neural networks, Meas. Sci. Technol **27**, 095901 (2016).
[9] E. Kit, C. Hocut, D. Liberzon, and H. J. Fernando, Fine-scale turbulent bursts in stable atmospheric boundary layer in complex terrain, J. Fluid Mech. **833**, 745 (2017).
[10] A. Tsinober, E. Kit, and T. Dracos, Experimental investigation of the field of velocity gradients in turbulent flows, J. Fluid Mech. **242**, 169 (1992).
[11] R. H. Kraichnan, Eddy viscosity in two and three dimensions, J. Atmos. Sci. **33**, 1521 (1976).
[12] T. De Karman and L. Howarth, On the statistical theory of isotropic turbulence, Proc. R. Soc. London A **164**, 192 (1938).
[13] M. Nelkin, Universality and scaling in fully developed turbulence, Adv. Phys. **43**, 143 (1994).
[14] H. J. Fernando and E. R. Pardyjak, Field studies delve into the intricacies of mountain weather, Eos **94**, 313 (2013).
[15] H. J. Fernando, E. R. Pardyjak, S. Di Sabatino *et al.*, The MATERHORN: Unraveling the intricacies of mountain weather, Bull. Am. Meteorol. Soc. **96**, 1945 (2015).

[16] E. Kit, A. Cherkassky, T. Sant, and H. S. Fernando, In situ calibration of hot-film probes using a collocated sonic anemometer: Implementation of a neural network, J. Atmos. Ocean. Tech. **27**, 23 (2010).
[17] T. Gotoh, D. Fukayama, and T. Nakano, Velocity field statistics in homogeneous steady turbulence obtained using a high-resolution direct numerical simulation, Phys. Fluids **14**, 1065 (2002).
[18] S. Sukoriansky, B. Galperin, and I. Staroselsky, Cross-term and ε-expansion in RNG theory of turbulence, Fluid Dyn. Res. **33**, 319 (2003).
[19] S. Sukoriansky, B. Galperin, and I. Staroselsky, A quasinormal scale elimination model of turbulent flows with stable stratification, Phys. Fluids **17**, 085107 (2005).
[20] F. K. Chow, R. L. Street, M. Xue, and J. H. Ferziger, Explicit filtering and reconstruction turbulence modeling for large-eddy simulation of neutral boundary layer flow, J. Atmos. Sci. **62**, 2058 (2005).
[21] P. P. Sullivan, T. W. Horst, D. H. Lenschow, C. Moeng, and J. C. Weil, Structure of subfilter-scale fluxes in the atmospheric surface layer with application to large-eddy simulation modelling, J. Fluid Mech. **482**, 101 (2003).
[22] A. Yakhot, S. A. Orszag, V. Yakhot, and M. Israeli, Renormalization group formulation of large-eddy simulations, J. Sci. Comput. **4**, 139 (1989).
[23] D. Forster, D. R. Nelson, and M. J. Stephen, Large-distance and long-time properties of a randomly stirred fluid, Phys. Rev. A **16**, 732 (1977).
[24] L. M. Smith and S. L. Woodruff, Renormalization-group analysis of turbulence, Annu. Rev. Fluid Mech. **30**, 275 (1998).
[25] V. Yakhot and S. A. Orszag, Renormalization group analysis of turbulence. I. Basic theory, J. Sci. Comput. **1**, 3 (1986).
[26] Y. Zhou, Renormalization group theory for fluid and plasma turbulence, Phys. Rep. **488**, 1 (2010).
[27] S. Sukoriansky and B. Galperin, QNSE theory of turbulence anisotropization and onset of the inverse energy cascade by solid body rotation, J. Fluid Mech. **805**, 384 (2016).
[28] S. Sukoriansky and E. Zemach, Theoretical study of anisotropic MHD turbulence with low magnetic Reynolds number, Phys. Scr. **91**, 034001 (2016).
[29] S. A. Orszag, Lectures on the statistical theory of turbulence, MIT, http://pordlabs.ucsd.edu/rsalmon/Orszag.1977.pdf (1974).
[30] P. Tabeling, G. Zocchi, F. Belin, J. Maurer, and H. Willaime, Probability density functions, skewness, and flatness in large Reynolds number turbulence, Phys. Rev. E **53**, 1613 (1996).
[31] C. W. Van Atta and R. A. Antonia, Reynolds number dependence of skewness and flatness factors of turbulent velocity derivatives, Phys. Fluids **23**, 252 (1980).
[32] A. Gylfason, S. Ayyalasomayajula, and Z. Warhaft, Intermittency, pressure and acceleration statistics, J. Fluid Mech. **501**, 213 (2004).
[33] F. Belin, J. Maurer, P. Tabeling, and H. Willaime, Velocity gradient distributions in fully developed turbulence, Phys. Fluids **9**, 3843 (1997).
[34] F. Belin, P. Tabeling, and H. Willaime, Exponents of the structure functions in a low temperature helium experiment, Physica D **93**, 52 (1996).
[35] P. A. Davidson and B. R. Pearson, Identifying Turbulent Energy Distributions in Real, Rather than Fourier, Space. Phys. Rev. Lett. **95**, 214501 (2005).
[36] S. Garg and Z. Warhaft, On the small scale structure of simple shear flow, Phys. Fluids **10**, 662 (1998).
[37] X. Shen and Z. Warhaft, The anisotropy of the small scale structure in high Reynolds number (R$\lambda\sim$ 1000) turbulent shear flow, Phys. Fluids **12**, 2976 (2000).